HHS Public Access

Author manuscript

Bone. Author manuscript; available in PMC 2016 June 01.

Published in final edited form as:

Bone. 2015 June ; 75: 120–127. doi:10.1016/j.bone.2015.01.021.

Inhibition of CaMKK2 Reverses Age-Associated Decline in Bone Mass

Zachary J. Pritchard[1], **Rachel L. Cary**[2], **Chang Yang**[3], **Deborah V. Novack**[3], **Michael J. Voor**[4,5,*], and **Uma Sankar**[1,2,6,*]

[1]Department of Pharmacology and Toxicology, University of Louisville School of Medicine, Louisville, KY

[2]James Graham Brown Cancer Center and Owensboro Cancer Research Program, University of Louisville School of Medicine, Louisville, KY

[3]Department of Medicine and Pathology, Washington University School of Medicine, St. Louis, MO

[4]Department of Orthopaedic Surgery, University of Louisville School of Medicine, Louisville, KY

[5]Department of Bioengineering, University of Louisville Speed School of Engineering, Louisville, KY

[6]Department of Anatomy and Cell Biology, Indiana University School of Medicine, Indianapolis, IN

Abstract

Decline in bone formation is a major contributing factor to the loss of bone mass associated with aging. We previously showed that the genetic ablation of the tissue-restricted and multifunctional Ca^{2+}/calmodulin (CaM)-dependent protein kinase kinase 2 (CaMKK2) stimulates trabecular bone mass accrual, mainly by promoting anabolic pathways and inhibiting catabolic pathways of bone remodeling. In this study, we investigated whether inhibition of this kinase using its selective cell-permeable inhibitor STO-609 will stimulate bone formation in 32 week old male WT mice and reverse age-associated of decline in bone volume and strength. Tri-weekly intraperitoneal injections of saline or STO-609 (10 μM) were performed for six weeks followed by metabolic labeling with calcein and alizarin red. New bone formation was assessed by dynamic histomorphometry whereas micro-computed tomography was employed to measure trabecular bone volume, microarchitecture and femoral mid-shaft geometry. Cortical and trabecular bone biomechanical properties were assessed using three-point bending and punch compression methods respectively. Our results reveal that as they progress from 12 to 32 weeks of age, WT mice sustain a significant decline in trabecular bone volume, microarchitecture and strength as well as cortical bone strength. However, treatment of the 32 week old WT mice with STO-609

[*]Address correspondences to: Uma Sankar, Ph.D., Department of Anatomy and Cell Biology, Indiana University Purdue University Indianapolis, 635 Barnhill Drive, MS-5055, Indianapolis, IN 46202 USA. Tel: (317) 274-7870, Fax: (317) 856-5710; usankar@iupui.edu; or Michael J. Voor, Ph.D., Orthopaedic Bioengineering Laboratory, University of Louisville, 40292 USA. Tel: (502) 852-7067, Fax: (502) 852-7227, michael.voor@louisville.edu..

stimulated apposition of new bone and completely reversed the age-associated decrease in bone volume, quality, as well as trabecular and cortical bone strength. We also observed that regardless of age, male *Camkk2*$^{-/-}$ mice possessed significantly elevated trabecular bone volume, microarchitecture and compressive strength as well as cortical bone strength compared to age-matched WT mice, implying that the chronic loss of this kinase attenuates age-associated decline in bone mass. Further, whereas STO-609 treatment and/or the absence of CaMKK2 significantly enhanced the femoral midshaft geometry, the midshaft cortical wall thickness and material bending stress remained similar among the cohorts, implying that regardless of treatment, the material properties of the bone remain similar. Thus, our cumulative results provide evidence for the pharmacological inhibition of CaMKK2 as a bone anabolic strategy in combating age-associated osteoporosis.

Graphical abstract

Keywords

Ca^{2+}/calmodulin (CaM)-dependent protein kinase kinase 2; STO-609; bone volume; trabecular punch compression; three-point bending; microarchitecture; mid-shaft cross-sectional area moment of inertia; osteoblasts

Introduction

The ubiquitous second messenger Ca^{2+} connects extracellular signals to intracellular biological processes [1, 2]. Ligand-receptor interactions at the cell surface generate intracellular Ca^{2+} transients that are immediately recognized by the highly conserved calmodulin (CaM). The resulting Ca^{2+}/CaM complex binds to and activates a host of downstream targets including the multifunctional Ca^{2+}/CaM-dependent protein kinases (CaMKs) [3]. CaMKs are a family of serine/threonine protein kinases that includes CaMKI, CaMKII and CaMKIV [2, 4, 5]. Of these, CaMKII is fully activated through autophosphorylation following Ca^{2+}/CaM binding. The other two family members CaMKI and CaMKIV require phosphorylation of an activation-loop threonine by two upstream kinases CaMKK1 (α) and CaMKK2 (β). The resulting CaMK signaling cascade has important functions in cell cycle, cell differentiation, adaptive and innate responses by immune cells, thymocyte survival, hematopoietic stem cell homeostasis, cerebellar granular cell differentiation, axon guidance, learning and memory [4-15]. More recently, adenosine mono-phosphate activated protein kinase (AMPK), a protein that coordinates cellular energy balance was identified as the third substrate of CaMKK2 [1, 16]. CaMKK2 is tissue-restricted and its loss protects mice from diet-induced obesity, insulin resistance and inflammatory responses [16-18].

We recently reported that CaMKK2 is expressed in osteoblasts (OBs) and osteoclasts (OCs) and that mice lacking this kinase possess enhanced trabecular bone mass in their long bones, along with significantly elevated numbers of OBs and fewer multinuclear OCs [19]. Moreover, pharmacological inhibition of CaMKK2 activity using its selective, cell-permeable pharmacological inhibitor STO-609 stimulated OB differentiation while inhibiting OC differentiation in vitro [19, 20]. Furthermore, STO-609 treatment protected 10 week-old mice from ovariectomy-induced bone loss by stimulating OBs and inhibiting OCs in vivo [19]. Collectively, our initial studies demonstrated that the loss of CaMKK2 strongly favors the anabolic pathways of remodeling and that its pharmacological inhibition protects mice from post-menopausal osteoporosis.

In the present study, we wanted to extend these observations by evaluating whether pharmacological inhibition of CaMKK2 will reverse age-related decline in bone mass, which occurs mainly due to decreased bone formation by OBs, rather than an increase in bone resorption [21]. Similar to humans, the trabecular bone volume in male C57BL6 mice declines continuously from 1.5 months to 24 months of age and the most rapid decline is observed between 6 to 12 months of age [22, 23]. Accordingly, we surmised that the acute inhibition of CaMKK2 using STO-609 would trigger new bone formation and reverse the age-associated loss of trabecular bone volume suffered by male C57BL6 mice at 32 weeks or 8 months of age. We also investigated whether the age-associated decline in trabecular bone microarchitecture as well as weakening of trabecular and cortical bone biomechanical strength are rescued following STO-609 treatment of 32 week old mice.

Materials and Methods

Mice

Male WT and *Camkk2*$^{-/-}$ mice (C57BL6 background) were housed in the University of Louisville (UofL) Baxter II Vivarium under a 12-h light, 12-h dark cycle. Food and water were provided *ad libitum*. All care and experimental procedures were performed according to UofL Institutional Animal Care and Use Committee protocols and in compliance with NIH guidelines on the use and care of laboratory and experimental animals.

Reagents and treatments

STO-609 was purchased from TOCRIS Bioscience (Ellsville, MO, USA) and prepared as mentioned previously [19]. Tri-weekly intraperitoneal (i.p.) injections of 200 μl per mouse of either saline (n=9) or 10 μM STO-609 (n=9) were administered into 32 week old WT mice for 6 weeks. Seven and two days before euthanasia, the saline (n=5) and STO-609 treated mice (n=8) were injected via i.p. with calcein (5 mg/ml) and alizarin red (15 mg/ml) respectively, at 100 μl per mouse. Long bones were harvested; tibiae were utilized for dynamic histomorphometry and femurs were utilized for microcomputed tomography (μCT) and mechanical testing. Microarchitecture analyses as well as assessment of both cortical and trabecular bone strength were performed. Untreated 12 week old WT (n=11) and *Camkk2*$^{-/-}$ (n=11) mice as well as 32 week old *Camkk2*$^{-/-}$ mice (n=6) were used as controls for μCT and strength analyses.

Dynamic bone histomorphometry and polarizing microscopy

Undecalcified histology and dynamic histomorphometry were performed on tibiae that were fixed in 70% ethanol. Longitudinal sections of the tibiae (10 μm) were prepared and new bone formation was assessed by fluorescence microscopy of calcein (green) and alizarin red (red). The region of interest was the metaphyseal bone covering 3.0 mm beneath the growth plate [24]. Histomorphometric analysis was performed by a blinded observer using BioQuant OSTEO 2010 software (BioQuant Image Analysis Corporation) and standard parameters [25]. The sections were subsequently stained with picrosirius red and imaged using polarizing microscopy to visualize spatial distribution of collagen fibers in bone [26].

Micro-CT Imaging

Micro-computed tomography (μCT) imaging was performed on a high resolution CT scanner (Actis HR225-150; BIR, Lincolnshire, IL, USA) located at the University of Louisville Orthopaedic Bioengineering Lab. Up to 3 femurs were imaged simultaneously at an isotropic voxel size of 7 μm. Transverse images of femurs covering a length of approximately 5.25 mm were processed individually for each femur using a combination of two-dimensional (ImageJ, NIH Image, Bethesda, MD) and three-dimensional (VG Studio Max, Volume Graphics, Heidelberg, DE) imaging software. We cropped a box-shaped volume of interest (VOI) approximately 2.0 × 1.0 × 0.75 mm from this stack of images. The VOI was located within the distal femoral metaphysis extending to within 100 μm of the proximal side of the distal femoral physis. After using a 2 × 2 Gaussian filter and a histogram based single gray-level threshold to segment cortical and cancellous bone tissue from background and soft tissue, trabecular architectural properties including bone volume fraction (BV/TV), trabecular thickness (Tb.Th), trabecular separation (Tb.Sp) and trabecular number (Tb.N) were determined for a standardized region in the distal femoral metaphysis. Mid-shaft geometry was calculated by measuring the mediolateral and anterior-posterior inner and outer diameters of the mid-diaphysis from the μCT images and calculating the cross-sectional area MOI and cortical bone thickness from these measurements using an elliptical cross-section assumption.

Mechanical testing

After the femurs were imaged in the μCT scanner, they were prepared for testing to determine cortical bone mechanical properties using three-point bending and cancellous bone mechanical properties using a flat-tipped cylindrical punch. The femurs were kept moist by wrapping in saline soaked gauze from the time of collection up to the time of testing. A servohydraulic load frame equipped with a 500 N capacity load cell with a sensitivity of 0.2 N was used for both mechanical tests (Model 858 Bionix, MTS Corp., Eden Prairie, MN).

Three-point-bending was performed by placing the femur across an 8 mm wide support span and loading vertically with a rounded knife edge at the center of the span contacting the posterior surface of the femoral diaphysis. The loading was applied at a displacement rate of 1 mm/min until the femur failed. The amount of force, F (N), applied was recorded and the

magnitude of the bending moment at the point of failure was calculated as:

$$M = \left[\frac{1}{4} * F * \text{support width}\right] \quad (N * mm).$$

Following the three-point bending test, the distal portion of the same femur was prepared for a punch-type compression test to measure the strength of the cancellous bone material in the distal part of the femoral metaphysis. To perform this test in mice, we modified a procedure outlined by An et al. for flat head indentation of the distal femur cancellous bone in rats [27]. The thickness of the epiphysis and distance to the base of the epiphyseal plate was measured for individual bones using μCT image analysis. This information was employed to trim the distal femurs to expose the base of the epiphyseal plates for precise indentation (Figure 3Ci). Briefly, the distal femur was mounted in the head of a #10 cap screw using two-part epoxy with the condyles exposed and the shaft of the femur oriented along the axis of the screw. The screw was mounted in a low-speed diamond sectioning saw and the blade was advanced to coincide with the position of the epiphysis as observed on μCT images taken previously. The end of the femur was trimmed, exposing the sub-epiphyseal cancellous bone of the distal metaphysis (Figure 3Ci). Then the screw/bone combination was positioned and centered under a 1 mm diameter flat-tipped cylindrical punch fixed to the actuator of the MTS machine. The flat 1 mm diameter punch tip was utilized and it produced approximately 1.27 MPa of compressive/contact stress for every 1 N of force applied. The tip was advanced at a rate of 1mm/min. The displacement and compressive force were recorded. Most importantly, the analysis of the data collected was limited to a depth of penetration of less than 1.5 mm to avoid high loads associated with contact of the punch tip with the cortical wall of the distal metaphysis.

Equations Used with Mechanical Testing

The maximum applied load in each type of test can be used as a measure of the cortical and cancellous bone strength, but to determine the true tissue strength, some normalization is required. The three-point-bending failure moment was converted to a maximum tissue stress using the following equation: $\sigma_b = \frac{My}{I}$; where σ_b represents stress (in MPa) of the femoral cortical bone tissue, M represents the maximum applied bending moment (in N•mm), y represents the vertical distance from the bone axis to the failure surface (in mm),and I represents the cross-sectional area moment of inertia (in mm^4; MOI), a geometric property of a beam that defines its resistance to bending. For blunt indentation, the applied compressive stress, σ_c was determined by the amount of applied force (F) divided by the cross-sectional area of the 1 mm diameter indenter tip (A): $\sigma_c = F/A$.

Statistical analysis

All data are represented as average values ± standard deviation. Statistical comparisons among untreated (12 week old), saline (WT) and STO-609 treated samples (32 week old) and *Camkk2*$^{-/-}$ (12 and 32 weeks of age) samples were performed by single factor ANOVA. Post-hoc *t*-test corrected using the Bonferroni method was utilized for multiple pair-wise comparisons. Differences with *p*-value < 0.05 were deemed significant.

Results

STO-609 stimulates bone formation in 32 week old adult mice

As a first step towards understanding whether inhibition of CaMKK2 will reverse age-associated bone loss, we evaluated if STO-609 treatment will trigger new bone formation in 32 week old WT mice, at an age where the trabecular bone mass in C57BL6 mice begins to decline [21]. Dynamic histomorphometry measurements of undecalcified sections (Figure 1Ai) indicated increases in mineral apposition rate (MAR; +13%; $p = 0.04$) and bone formation rate (BFR; +40%; $p = 0.009$) following the acute pharmacological inhibition of CaMKK2 in 32 week old mice (Figures 1B-C). Further, dense lamellar structures were visible in picrosirius stained femur sections from STO-609-treated mice when visualized under polarized light (Figure 1Aii).

CaMKK2 inhibition elicits trabecular bone mass accrual in 32 week old mice

Next, to understand the extent of bone loss suffered by mice as they aged, we evaluated trabecular bone volume in the distal femurs of 12 and 32 week old WT and *Camkk2*$^{-/-}$ mice using μCT analysis. In accordance with our previous data in 8 week old female mice [19], we found the 12 week old *Camkk2*$^{-/-}$ mice to possess 1.7-fold higher BV/TV than age-matched WT mice (Figures 2A and 2B; $p = 0.00004$). Interestingly, this difference was more pronounced in the aged mice, such that the 32 week old *Camkk2*$^{-/-}$ mice possessed 2.4 fold higher BV/TV than age-matched WT cohorts ($p = 0.000001$), suggesting a higher amount of age-associated bone loss in WT mice. Accordingly, as shown in Figure 2B, whereas the WT mice suffered a 39% decline in trabecular bone volume from 12 to 32 weeks ($p = 0.001$), the bone loss over the same time period in *Camkk2*$^{-/-}$ mice was an insignificant 11% ($p = 0.22$). We then asked whether the acute inhibition of CaMKK2 through a six week regimen of tri-weekly STO-609 administration will reverse the age-associated bone loss in 32 week old WT mice. Indeed, treatment of 32 week old WT mice with STO-609 resulted in a 1.7-fold increase in trabecular bone volume fraction compared to saline treated WT controls ($p = 0.0006$). Notably, BV/TV of STO-609 treated 32 week old mice was comparable to that of untreated 12 week old WT mice (Figure 2 A-B; $p = 0.62$).

Trabecular bone microarchitecture improves in 32 week old mice following STO-609 treatment

Next we compared the microarchitecture parameters of the trabecular bone among the 12 and 32 week WT and *Camkk2*$^{-/-}$ mouse cohorts as well as the STO-609 treated 32 week old WT mice. Consistent with the BV/TV measurements, trabecular number (Tb.N) in 12 week old *Camkk2*$^{-/-}$ mice was 1.4-fold higher than age-matched WT mice ($p = 0.00006$), and this difference was exacerbated to 1.9 fold between the 32 week old cohorts (Figure 2C; $p = 0.000002$). Whereas WT mice sustained a 34% decrease in Tb.N. as they aged from 12 to 32 weeks of age ($p = 0.0001$), the comparable loss of Tb.N in *Camkk2*$^{-/-}$ over the same time period was only 8% (Figure 2C; $p = 0.2$). Remarkably, treatment of 32 week old WT mice with STO-609 resulted in an increase in Tb.N by 26% ($p = 0.03$), such that the trabecular number in these mice were similar to that in untreated 12 week old mice (Figure 2C).

Trabecular separation (Tb.Sp) in these mouse cohorts closely followed the trends observed for BV/TV and Tb.N. Whereas, trabecular separation did not increase significantly in *Camkk2*$^{-/-}$ mice as they aged from 12 to 32 weeks ($p = 0.2$), WT mice sustained a 63% increase in trabecular spacing over the same time period (Figure 2D; $p = 0.0002$). STO-609 treatment reversed this trend by decreasing Tb.Sp by 41% ($p = 0.0005$) and bringing it closer to the value observed in untreated 12 week old WT mice (Figure 2D; $p = 0.6$). Remarkably, Tr.Sp remained markedly lower in *Camkk2*$^{-/-}$ mice, compared to WT, no matter the age. Thus, the *Camkk2*$^{-/-}$ mice possessed 1.7-fold ($p = 0.00002$) and 2.4-fold ($p = 0.00008$) lower Tb.Sp at 12 and 32 weeks of age, respectively, than age-matched WT cohorts.

We also observed similar trends in trabecular thickness. Tb.Th decreased by19% ($p = 0.01$) in 32 week old WT mice compared to the 12 week old cohorts, whereas this decrease was rescued by STO-609 treatment. Thus, Tb.Th increased by 26% ($p = 0.001$) in 32 week old mice following STO-609 treatment, such that it was similar to what was observed in 12 week old WT mice (Figure 2E; $p = 0.2$). Here again, we observed higher Tb.Th. in 12 and 32 week old *Camkk2*$^{-/-}$ mice compared to age-matched WT mice, and did not observe a significant decrease in this parameter as the mutant mice aged from 12 to 32 weeks (Figure 2E; $p = 0.2$).

CaMKK2 inhibition improves trabecular and cortical bone strength in older mice

We further analyzed the cortical bone strength in these mice by using the three-point bending to failure method. Compared to 12 week old cohorts, femoral mid-shaft bending strength decreased by 18% in 32 week old WT mice ($p = 0.02$). However, this decline in cortical bone strength in older animals was rescued by STO-609 treatment such that femurs from drug-treated mice possessed 21% higher mid-shaft bending strength, compared to saline-treated 32 week old WT mice (Figure 3A; $p = 0.006$). The three-point bending strength in 12 week old *Camkk2*$^{-/-}$ mice was 1.4-fold higher than in age-matched WT mice ($p = 0.0008$). Interestingly, *Camkk2*$^{-/-}$ mice suffered a 25% age-dependent decline in cortical bone bending strength from 12 to 32 weeks of age (59.4 ± 8.3 N•mm at 12 weeks vs. 45 ± 3.8 N•mm at 32 weeks; $p = 0.002$). However, the femoral mid-shaft bending strength of 32 week old *Camkk2*$^{-/-}$ mice was still higher than 32 week old WT mice (Figure 3A; $p = 0.01$).

Next, we tested the biomechanical properties and strength of the trabecular bone accumulated by older mice in their distal femurs following a 6-week treatment of STO-609 or present in enhanced quantities in young and old *Camkk2*$^{-/-}$ mice. Direct blunt punch compressive strength of trabecular bone diminished by 18% as WT mice aged from 12 to 32 weeks ($p = 0.02$). However, following treatment with STO-609, the compressive strength of trabecular bone in the 32 week old animals increased by 34% (Figure 3Cii; $p = 0.0004$). Interestingly, trabecular bone strength of STO-609 treated older mice was higher than that of 12 week old mice ($p = 0.007$), suggesting that CaMKK2 inhibition in 32 week old animals stimulated the formation of trabecular bone with strength that is superior to that in younger mice. Trabecular bone compressive strength in 12 week old *Camkk2*$^{-/-}$ mice was on average 1.7 fold higher than that in age-matched WT mice ($p = 0.00002$). Of note, although *Camkk2*$^{-/-}$ mice did suffer from an age-dependent decline in compressive strength of the

trabecular bone (48.4 ± 9 MPa at 12 weeks vs. 39.7 ± 7 MPa at 32 weeks of age), this decrease was insignificant ($p = 0.07$). Moreover, the breaking force of trabecular bone in the older *Camkk2*$^{-/-}$ mice was still higher (1.7-fold) than that in 32-week old saline-treated WT mice (Figure 3 Cii; $p = 0.0003$).

CaMKK2 inhibition enhances mid-shaft geometry in 32 week old WT mice

We next evaluated the femur mid-shaft geometry in these mouse cohorts. Our data show that aging from 12 weeks to 32 weeks resulted in a 29% decline ($p = 0.04$) in femur mid-shaft cross-sectional area MOI in WT mice (Table). This decline was rescued by treating 32 week old WT mice with STO-609 which elicited a 28% increase ($p = 0.03$) of mid-shaft cross-sectional area MOI (Table). Further, consistent with our previous observations, the mid-shaft geometry was enhanced in *Camkk2*$^{-/-}$ mice regardless of age. Thus, the 12 week old *Camkk2*$^{-/-}$ mice possessed 32% ($p = 0.008$) larger mid-shaft cross-sectional area MOI, compared to age-matched WT cohorts. Furthermore, although *Camkk2*$^{-/-}$ mice did sustain a 27% decline in the femur mid-diaphysis cross-sectional area from 12 to 32 weeks of age ($p = 0.02$), these parameters in the older *Camkk2*$^{-/-}$ mice were still a significant 34% higher ($p = 0.009$) than those in 32 week-old WT mice (Table). In contrast to this increase in the mid-shaft geometry associated with inhibition and/or loss of CaMKK2, we did not observe any differences in the cortical bone thickness among the cohorts (Table). Moreover, when the differences in cross-sectional area MOI were taken into account, the three-point bending stress was not significantly different among the mouse cohorts (Figure 3B).

Discussion

Age dependent decline in bone mass, microarchitecture and strength occurs in both men and women, which if left untreated increases the risk of fragility fractures [22, 28]. Decreased bone formation is a major contributing factor to this decline, and mechanisms that stimulate bone anabolism will enable the attenuation or even a reversal of this otherwise inevitable age-associated outcome. Our previous studies identified CaMKK2 as one such mechanism as its absence or pharmacological inhibition stimulates anabolic pathways and inhibits catabolic pathways of bone remodeling resulting in enhanced trabecular bone mass accrual [19]. Therefore, we hypothesized that the bone anabolic effect triggered by CaMKK2 inhibition will rescue the decline in bone volume and strength associated with normal aging in WT mice. Male mice were chosen for this study to avoid complications from estrous cycle and the related hormone-associated changes in bone remodeling as well as their impact on skeletal aging [29]. Moreover, previous studies do indicate age-associated decline in bone mass in male C57BL6 mice linked with decreased OB-mediated bone formation [21, 23]. Thus, in this study, we compared trabecular bone volume and microarchitecture as well as the biomechanical properties of the trabecular and cortical bone in WT and *Camkk2*$^{-/-}$ mice as well as STO-609-treated 32 week old WT mice.

Comparison of the measures of both cortical and cancellous bone from 12 and 32 week old WT mice show the natural history of age-dependent reduction in bone quality in mice. Thus, the WT mice suffered a significant decline in trabecular bone volume, decreased thickness and number, increased trabecular separation as well as diminished cortical and trabecular

bone strength as they progressed from 12 to 32 weeks of age. However, pharmacological inhibition of CaMKK2 completely reversed this age-associated decrease in these bone parameters. Accordingly, metabolic labeling studies indicate stimulation of bone apposition in the long bones of 32 week old WT mice following the acute inhibition of CaMKK2. Furthermore, treatment with STO-609 significantly increased trabecular bone volume, microarchitecture, strength as well as mid-shaft geometry and cortical bone strength in 32 week old mice to the levels observed in 12 week old WT mice. Moreover, regardless of age, the *Camkk2*$^{-/-}$ mice possessed significantly elevated trabecular bone volume fraction, trabecular thickness, trabecular number and compressive strength compared to age-matched WT mice. Furthermore, cortical bone geometry as well as femoral midshaft bone bending strength was significantly elevated in both 12 and 32 week old *Camkk2*$^{-/-}$ mice compared to WT. Although the *Camkk2*$^{-/-}$ mice did sustain smaller, and sometimes significant, age-associated decline in bone mass, quality and/or strength, these parameters were still significantly higher in 32 week old *Camkk2*$^{-/-}$ mice than age-matched WT mice, implying that the absence of CaMKK2 blunts the deleterious effects of aging on bone. Taken together, our data indicate that the inhibition of CaMKK2 using STO-609 reverses the age-associated loss of bone mass, microarchitecture and overall strength whereas its chronic absence in *Camkk2*$^{-/-}$ mice attenuates the deleterious effects of normal aging on bone (Figure 4).

Ultrastructural features of trabecular bone are optimized by bone remodeling, a process characterized by OC-induced bone resorption and OB-mediated bone formation [30]. Complete inhibition of OC activity results in higher bone volume, but leads to stiff and brittle bones that break or fracture more easily [31, 32]. On one hand, administration of antiresorptive therapies will inhibit age-induced bone loss and the accumulation of mechanical flaws. On the other hand, complete inhibition of OC activity with or without accompanying anabolic activity can result in an excessive accumulation of microdamage and hypermineralized regions, resulting in brittle bones that are prone to cracking [31, 33, 34]. Conversely, higher bone volumes and stronger bone can also be achieved through increased bone formation by stimulation of OBs without necessarily completely inhibiting OCs [31, 32]. Thus, the most ideal anti-osteoporosis therapies will stimulate OB-mediated anabolic activity while suppressing, but not completely eliminating OCs. In older individuals experiencing active bone remodeling, such a therapy will create a positive bone multicellular unit balance by stimulating the formation of new bone with superior architecture and biomechanical properties [35-37].

The lack of CaMKK2 favors OBs, but the *Camkk2*$^{-/-}$ long bones do possess OCs albeit at significantly decreased levels compared to WT [19]. Our cumulative μCT imaging and strength data from this study clearly suggest a renewed anabolic bone effect in adult mice following an acute pharmacological inhibition of CaMKK2 in 32 week old WT mice. In *Camkk2*$^{-/-}$ mice and STO-609 treated older mice, this anabolic effect is accompanied by superior trabecular bone quality and strength, resulting from the limited, but ongoing OC-mediated remodeling activity which maintains normal bone material properties at the tissue level. Further, imaging data for the cortical bone of the femoral shaft show that there was a significant anabolic effect of STO-609 on the cortical bone of older WT mice as the outer

mediolateral and anterior-posterior mid-shaft diameters were higher in these mice compared to age-matched controls.

Interestingly, the inner diameters also increased, indicating a continued activity of the OCs and endosteal bone resorption. However, the increased mid-shaft outer diameters in the STO-609 treated 32 week old mice show that this is compensated by increased periosteal apposition, resulting in stronger cortices with significantly increased cross-sectional area MOI.

The three-point-bending mechanical testing data support this premise because the overall femoral cortical bone bending strength was higher in STO-609 treated 32 week old WT and *Camkk2*$^{-/-}$ mice, but the tissue level strength was not different. Whereas the structural differences in cortical bone are significant, the overall material quality of bone among the cohorts is similar, as evidenced by similar cortical mid-shaft thickness and material bending stress. In other words, the net anabolic effects of CaMKK2 genetic ablation or pharmacological inhibition result in significantly higher breaking strength, but the continued remodeling by OCs, albeit reduced in numbers [19], helps maintain the newly formed bone at an overall material quality that is similar to that in untreated age-matched WT mice. Thus, it is likely that the resulting bone tissue is normal due to continued remodeling, as opposed to increased mineralization and brittleness often seen with bisphosphonate therapy and osteopetrosis [38-40].

Both trabecular and cortical components of the bone are involved in fragility fractures that are a major consequence of age-associated bone loss [41, 42]. Bridges formed by trabecular bone in the metaphysis of long bones reinforce the surrounding cortical bone and enable the even distribution of load from the joints to the predominantly cortical diaphysis [42-44]. Diminished OB activity associated with aging contributes to thinner and fewer trabeculae resulting in a loss of trabecular microarchitecture [42]. The consequent failure of the trabecular reinforcement of the inner cortical bone surface triggers cortical bone porosity, ultimately increasing the risk of fragility factures such as those involving the distal radius, distal tibia and proximal femur [42, 43]. Bone anabolic activity stimulated in older mice by the acute inhibition of CaMKK2 significantly improves trabecular microarchitecture while enhancing cortical bone geometry. The accompanying reduced level of OC-mediated remodeling activity [19] imparts the newly formed bone with higher strength. More importantly, the fact that STO-609 administration stimulated OB-mediated bone formation in older 32 week old WT mice, completely reversing the age-associated bone loss observed in untreated older mice, demonstrates the potential utility of therapeutically inhibiting CaMKK2 to reverse bone loss while improving cortical and trabecular bone strength in patients at risk for age-associated fragility fractures.

Acknowledgements

The authors thank Dr. David Burr for a critical reading of the manuscript. This work was supported in part by grants from the American Cancer Society (RSG 13-301-01), Department of Defense/CDMRP (PR121604) and an intramural competitive enhancement grant from the Office of the Vice President for Research at the University of Louisville. DVN is supported by AR052705 (NIAMS). Dynamic histomorphometry and histological analysis was supported by The Center for Musculoskeletal Biology and Medicine at Washington University, P30AR057235 (NIAMS).

References

1. Racioppi L, Means AR. Calcium/Calmodulin-Dependent Protein Kinase Kinase 2: Roles in Signaling and Pathophysiology. J Biol Chem. 2012
2. Colomer J, Means AR. Physiological roles of the Ca2+/CaM-dependent protein kinase cascade in health and disease. Subcell Biochem. 2007; 45:169–214. [PubMed: 18193638]
3. Means AR. The Year in Basic Science: calmodulin kinase cascades. Molecular endocrinology. 2008; 22(12):2759–65. [PubMed: 18845671]
4. Kitsos CM, Sankar U, Illario M, Colomer-Font JM, Duncan AW, Ribar TJ, Reya T, Means AR. Calmodulin-dependent protein kinase IV regulates hematopoietic stem cell maintenance. The Journal of biological chemistry. 2005; 280(39):33101–8. [PubMed: 16020540]
5. Kokubo M, Nishio M, Ribar TJ, Anderson KA, West AE, Means AR. BDNF-mediated cerebellar granule cell development is impaired in mice null for CaMKK2 or CaMKIV. J Neurosci. 2009; 29(28):8901–13. [PubMed: 19605628]
6. Anderson KA, Means AR. Defective signaling in a subpopulation of CD4(+) T cells in the absence of Ca(2+)/calmodulin-dependent protein kinase IV. Mol Cell Biol. 2002; 22(1):23–9. [PubMed: 11739719]
7. Anderson KA, Means RL, Huang QH, Kemp BE, Goldstein EG, Selbert MA, Edelman AM, Fremeau RT, Means AR. Components of a calmodulin-dependent protein kinase cascade. Molecular cloning, functional characterization and cellular localization of Ca2+/calmodulin-dependent protein kinase kinase beta. J Biol Chem. 1998; 273(48):31880–9. [PubMed: 9822657]
8. Anderson KA, Ribar TJ, Illario M, Means AR. Defective survival and activation of thymocytes in transgenic mice expressing a catalytically inactive form of Ca2+/calmodulin-dependent protein kinase IV. Mol Endocrinol. 1997; 11(6):725–37. [PubMed: 9171236]
9. Cipolletta E, Monaco S, Maione AS, Vitiello L, Campiglia P, Pastore L, Franchini C, Novellino E, Limongelli V, Bayer KU, Means AR, Rossi G, Trimarco B, Iaccarino G, Illario M. Calmodulin-dependent kinase II mediates vascular smooth muscle cell proliferation and is potentiated by extracellular signal regulated kinase. Endocrinology. 2010; 151(6):2747–59. [PubMed: 20392834]
10. Illario M, Giardino-Torchia ML, Sankar U, Ribar TJ, Galgani M, Vitiello L, Masci AM, Bertani FR, Ciaglia E, Astone D, Maulucci G, Cavallo A, Vitale M, Cimini V, Pastore L, Means AR, Rossi G, Racioppi L. Calmodulin-dependent kinase IV links Toll-like receptor 4 signaling with survival pathway of activated dendritic cells. Blood. 2008; 111(2):723–31. [PubMed: 17909078]
11. Racioppi L, Means AR. Calcium/calmodulin-dependent kinase IV in immune and inflammatory responses: novel routes for an ancient traveller. Trends in immunology. 2008; 29(12):600–7. [PubMed: 18930438]
12. Ribar TJ, Rodriguiz RM, Khiroug L, Wetsel WC, Augustine GJ, Means AR. Cerebellar defects in Ca2+/calmodulin kinase IV-deficient mice. J Neurosci. 2000; 20(22):RC107. [PubMed: 11069976]
13. Wu JY, Gonzalez-Robayna IJ, Richards JS, Means AR. Female fertility is reduced in mice lacking Ca2+/calmodulin-dependent protein kinase IV. Endocrinology. 2000; 141(12):4777–83. [PubMed: 11108293]
14. Wu JY, Means AR. Ca(2+)/calmodulin-dependent protein kinase IV is expressed in spermatids and targeted to chromatin and the nuclear matrix. J Biol Chem. 2000; 275(11):7994–9. [PubMed: 10713118]
15. Zhang X, Wheeler D, Tang Y, Guo L, Shapiro RA, Ribar TJ, Means AR, Billiar TR, Angus DC, Rosengart MR. Calcium/calmodulin-dependent protein kinase (CaMK) IV mediates nucleocytoplasmic shuttling and release of HMGB1 during lipopolysaccharide stimulation of macrophages. Journal of immunology. 2008; 181(7):5015–23.
16. Anderson KA, Ribar TJ, Lin F, Noeldner PK, Green MF, Muehlbauer MJ, Witters LA, Kemp BE, Means AR. Hypothalamic CaMKK2 Contributes to the Regulation of Energy Balance. Cell Metabolism. 2008; 7(5):377–388. [PubMed: 18460329]
17. Racioppi L, Noeldner PK, Lin F, Arvai S, Means AR. Calcium/Calmodulin-dependent Protein Kinase Kinase 2 Regulates Macrophage-mediated Inflammatory Responses. J Biol Chem. 2012; 287(14):11579–91. [PubMed: 22334678]

18. Anderson KA, Lin F, Ribar TJ, Stevens RD, Muehlbauer MJ, Newgard CB, Means AR. Deletion of CaMKK2 from the liver lowers blood glucose and improves whole-body glucose tolerance in the mouse. Mol Endocrinol. 2012; 26(2):281–91. [PubMed: 22240810]
19. Cary RL, Waddell S, Racioppi L, Long F, Novack DV, Voor MJ, Sankar U. Inhibition of ca(2+)/calmodulin-dependent protein kinase kinase 2 stimulates osteoblast formation and inhibits osteoclast differentiation. J Bone Miner Res. 2013; 28(7):1599–610. [PubMed: 23408651]
20. Tokumitsu H, Inuzuka H, Ishikawa Y, Ikeda M, Saji I, Kobayashi R. STO-609, a specific inhibitor of the Ca(2+)/calmodulin-dependent protein kinase kinase. J Biol Chem. 2002; 277(18):15813–8. [PubMed: 11867640]
21. Ferguson VL, Ayers RA, Bateman TA, Simske SJ. Bone development and age-related bone loss in male C57BL/6J mice. Bone. 2003; 33(3):387–98. [PubMed: 13678781]
22. Clarke BL, Khosla S. Physiology of bone loss. Radiol Clin North Am. 2010; 48(3):483–95. [PubMed: 20609887]
23. Halloran BP, Ferguson VL, Simske SJ, Burghardt A, Venton LL, Majumdar S. Changes in bone structure and mass with advancing age in the male C57BL/6J mouse. J Bone Miner Res. 2002; 17(6):1044–50. [PubMed: 12054159]
24. Ramanadham S, Yarasheski KE, Silva MJ, Wohltmann M, Novack DV, Christiansen B, Tu X, Zhang S, Lei X, Turk J. Age-Related Changes in Bone Morphology Are Accelerated in Group VIA Phospholipase A2 (iPLA2β)-Null Mice. The American Journal of Pathology. 2008; 172(4): 868–881. [PubMed: 18349124]
25. Parfitt AM, Drezner MK, Glorieux FH, Kanis JA, Malluche H, Meunier PJ, Ott SM, Recker RR. Bone histomorphometry: standardization of nomenclature, symbols, and units. Report of the ASBMR Histomorphometry Nomenclature Committee. J Bone Miner Res. 1987; 2(6):595–610. [PubMed: 3455637]
26. Dziedzic-Goclawska A, Rozycka M, Czyba JC, Moutier R, Lenczowski S, Ostrowski K. Polarizing microscopy of Picrosirius stained bone sections as a method for analysis of spatial distribution of collagen fibers by optical diffractometry. Basic Appl Histochem. 1982; 26(4):227–39. [PubMed: 6187326]
27. An YH, Zhang J, Kang Q, Friedman RJ. Mechanical properties of rat epiphyseal cancellous bones studied by indentation testing. J Mater Sci Mater Med. 1997; 8(8):493–5. [PubMed: 15348716]
28. Khosla S. Pathogenesis of age-related bone loss in humans. J Gerontol A Biol Sci Med Sci. 2013; 68(10):1226–35. [PubMed: 22923429]
29. Manolagas SC, Bellido T, Jilka RL. Sex steroids, cytokines and the bone marrow: new concepts on the pathogenesis of osteoporosis. Ciba Found Symp. 1995; 191:187–96. discussion 197-202. [PubMed: 8582197]
30. Birkenhager-Frenkel DH, Nigg AL, Hens CJ, Birkenhager JC. Changes of interstitial bone thickness with age in men and women. Bone. 1993; 14(3):211–6. [PubMed: 8363859]
31. Turner CH. Bone strength: current concepts. Ann N Y Acad Sci. 2006; 1068:429–46. [PubMed: 16831941]
32. Seeman E. Bone quality: the material and structural basis of bone strength. J Bone Miner Metab. 2008; 26(1):1–8. [PubMed: 18095057]
33. Burr DB, Forwood MR, Fyhrie DP, Martin RB, Schaffler MB, Turner CH. Bone microdamage and skeletal fragility in osteoporotic and stress fractures. J Bone Miner Res. 1997; 12(1):6–15. [PubMed: 9240720]
34. Ruppel ME, Miller LM, Burr DB. The effect of the microscopic and nanoscale structure on bone fragility. Osteoporos Int. 2008; 19(9):1251–65. [PubMed: 18317862]
35. Grimston SK, Watkins MP, Stains JP, Civitelli R. Connexin43 modulates post-natal cortical bone modeling and mechano-responsiveness. Bonekey Rep. 2013; 2:446. [PubMed: 24422141]
36. Laurent M, Antonio L, Sinnesael M, Dubois V, Gielen E, Classens F, Vanderschueren D. Androgens and estrogens in skeletal sexual dimorphism. Asian J Androl. 2014; 16(2):213–22. [PubMed: 24385015]
37. Reeve J, Loveridge N. The fragile elderly hip: mechanisms associated with age-related loss of strength and toughness. Bone. 2014; 61:138–48. [PubMed: 24412288]

38. Sasaki H, Miyakoshi N, Kasukawa Y, Maekawa S, Noguchi H, Kamo K, Shimada Y. Effects of combination treatment with alendronate and vitamin K(2) on bone mineral density and strength in ovariectomized mice. J Bone Miner Metab. 2010; 28(4):403–9. [PubMed: 20101424]

39. Del Fattore A, Cappariello A, Teti A. Genetics, pathogenesis and complications of osteopetrosis. Bone. 2008; 42(1):19–29. [PubMed: 17936098]

40. Allen MR, Burr DB. Bisphosphonate effects on bone turnover, microdamage, and mechanical properties: what we think we know and what we know that we don't know. Bone. 2011; 49(1):56–65. [PubMed: 20955825]

41. Seeman E, Delmas PD. Bone quality--the material and structural basis of bone strength and fragility. N Engl J Med. 2006; 354(21):2250–61. [PubMed: 16723616]

42. Bala Y, Bui QM, Wang X, Iuliano S, Wang Q, Ghasem-Zadeh A, Rozental TD, Bouxsein ML, Zebaze R, Seeman E. Trabecular and Cortical Microstructure and Fragility of the Distal Radius in Women. J Bone Miner Res. 2014

43. Chen H, Kubo KY. Bone three-dimensional microstructural features of the common osteoporotic fracture sites. World J Orthop. 2014; 5(4):486–95. [PubMed: 25232524]

44. Tassani S, Matsopoulos GK. The micro-structure of bone trabecular fracture: An inter-site study. Bone. 2014; 60(0):78–86. [PubMed: 24334190]

Highlights

- CaMKK2 inhibition stimulates new bone formation in 32 week old mice.
- Inhibition CaMKK2 reverses age-associated loss of trabecular bone volume and microarchitecture.
- CaMKK2 inhibition by STO-609 rescues age-associated weakening in trabecular and cortical bone strength.
- Chronic absence of CaMKK2 in the knockout mice attenuates age-induced decline in bone volume and strength.

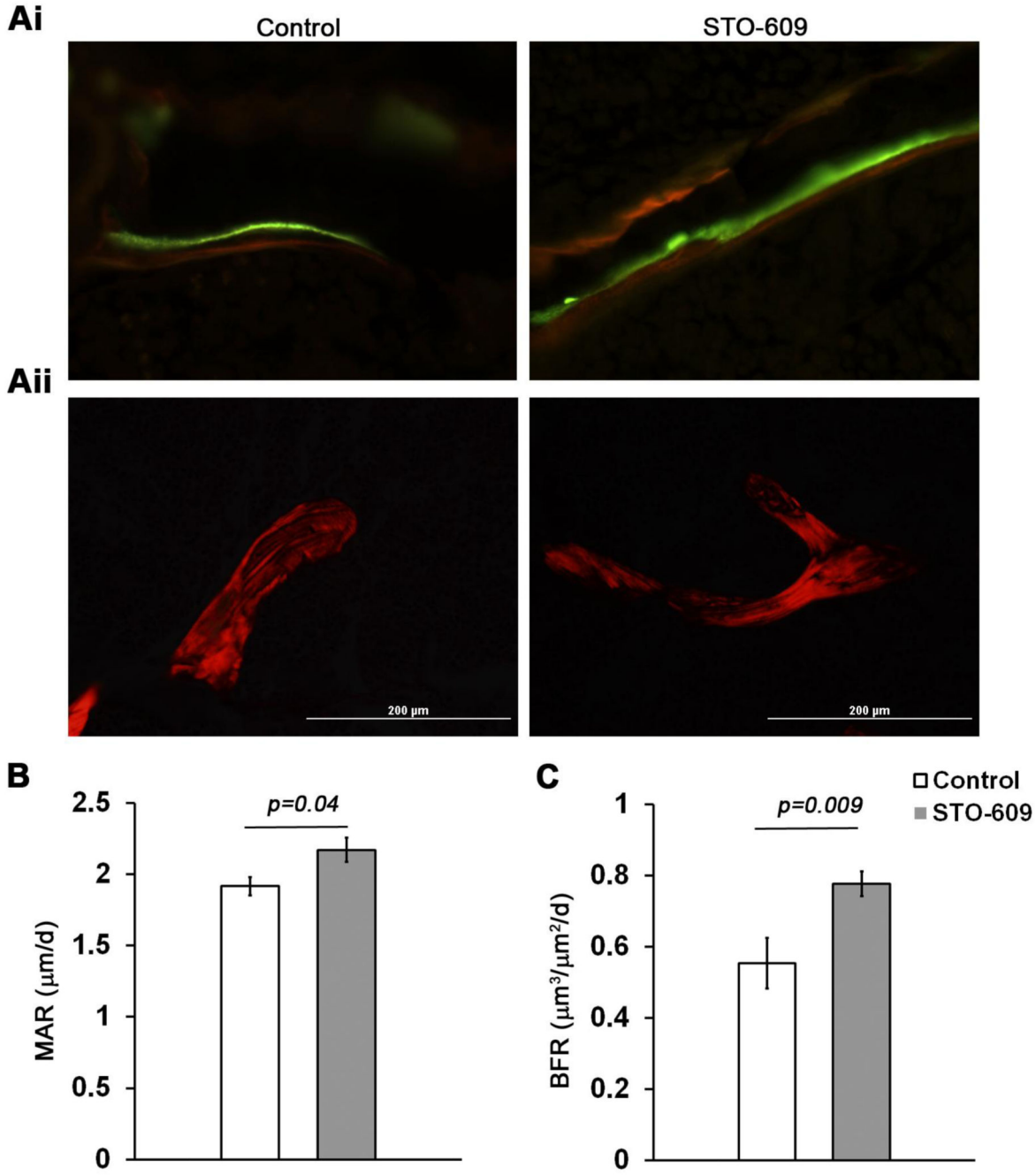

Figure 1. STO-609 administration stimulates trabecular bone formation in thirty-two week old mice

(Ai) Representative calcein and alizarin red-labelled sections of proximal tibiae from thirty-two week old mice that were administered saline or STO-609 for six weeks (400× magnification). **(Aii)** Representative digital polarized images of picrosirius red-stained methyl methacrylamide sections of proximal tibiae from saline or STO-609 treated mice (400× magnification). **(B-C)** Dynamic histomorphometry analysis of trabecular bone formation in proximal tibiae: mineral apposition rate (MAR) and bone formation rate (BFR).

Average values ± standard deviation from saline (n=5) and STO-609 treated (n=8) 32 week old WT mice are shown. Actual *p*-values are shown.

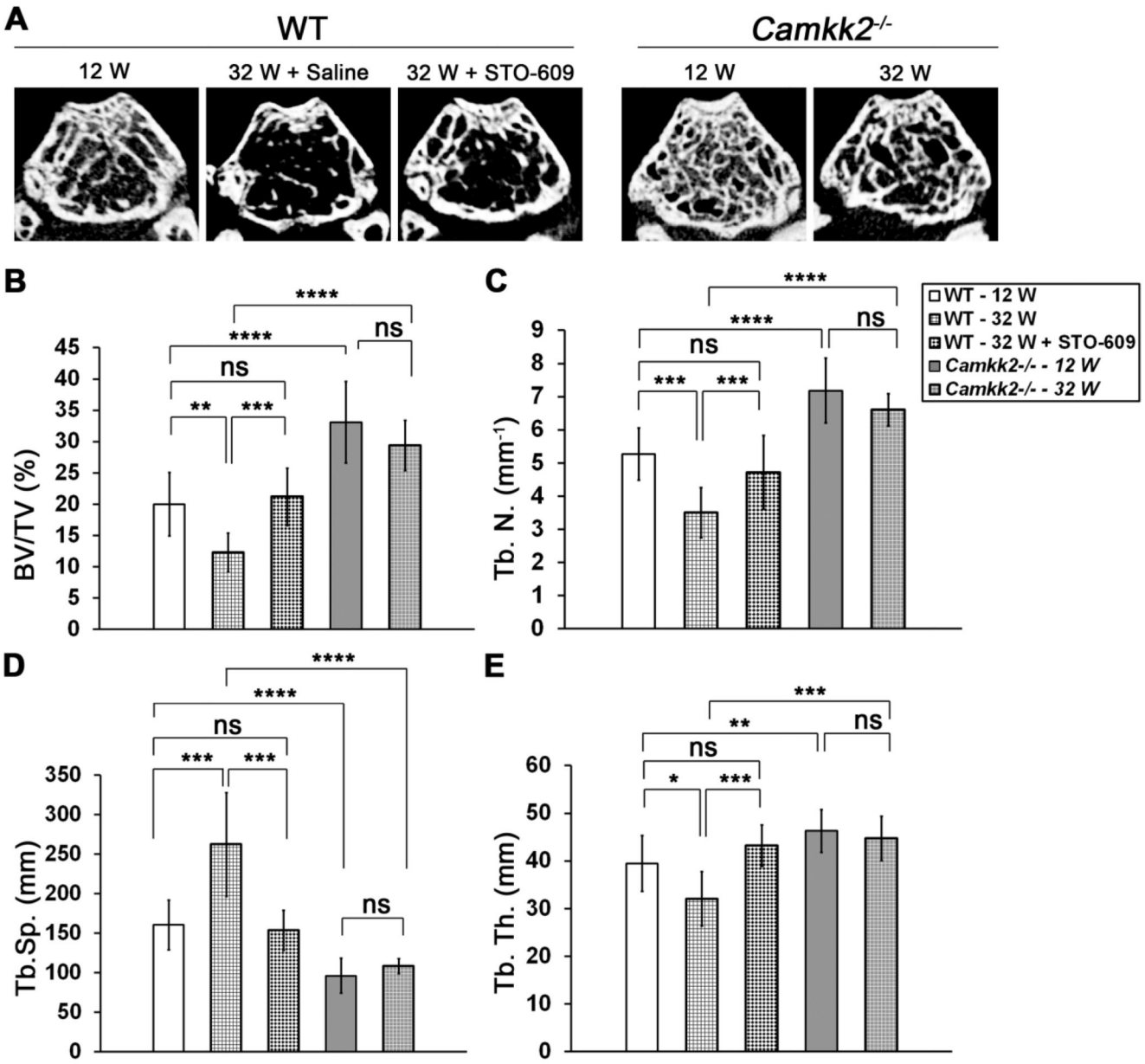

Figure 2. Effects of CaMKK2 inhibition or its genetic deletion on age-associated decline in trabecular bone volume and microarchitecture

(A) Representative digital μCT cross-sectional images of distal femurs from 12 week old (n=11 each for WT and *Camkk2*$^{-/-}$) and 32 week old (n=9 for WT and n=6 for *Camkk2*$^{-/-}$) WT and *Camkk2*$^{-/-}$ mice as well as STO-609 treated 32 week old (n=9) WT mice. **(B-D)** Average ± standard deviation μCT measurements of BV/TV (%), Tb.N (mm^{-1}), Tb.Sp. (μm) and Tb.Th. (μm) parameters from distal femurs of indicated cohorts are shown. Statistical comparisons among the cohorts were performed using single factor ANOVA followed by post-hoc *t*-test and Bonferroni correction for pair-wise comparisons. Differences with *p* - values < 0.05 were deemed significant and denoted as * = p<0.05; ** = p<0.01; *** = p<0.001 and **** = p<0.0001.

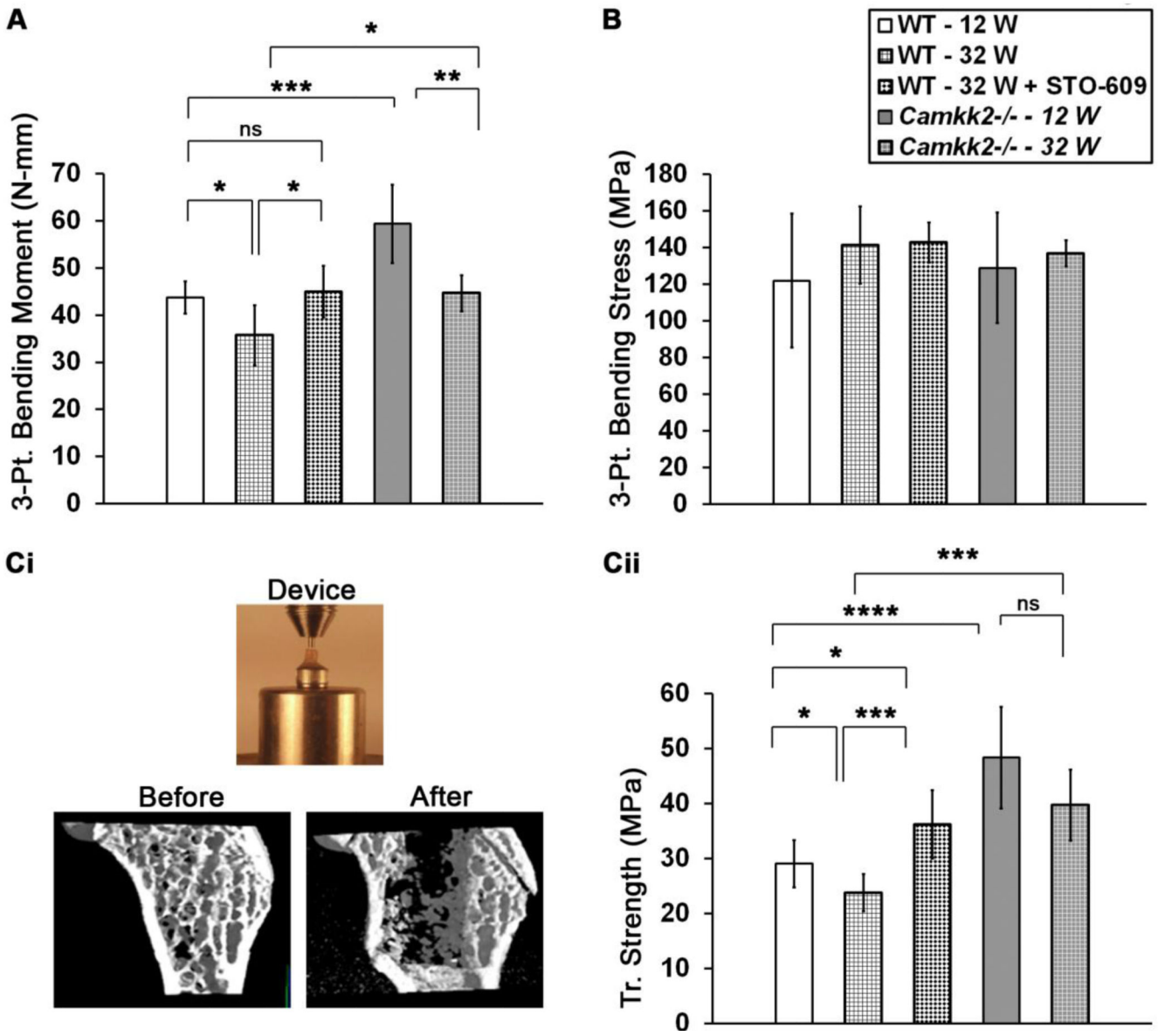

Figure 3. Higher trabecular and cortical bone strength in STO-609 treated 32 week old mice as well as 12 and 32 week old *Camkk2*$^{-/-}$ mice

(A) Average three-point bending moment ± standard deviation of the femoral mid-shaft indicating cortical bone strength from indicated cohorts in N.mm. **(B)** Three-point bending stress (average ± standard deviation) of the femoral mid-shaft indicating cortical bone material properties from indicated cohorts in MPa are shown. Bending stress was similar among all cohorts examined. **(C) (Top)** Digital photograph showing the direct blunt indentation device comprising a flat 1 mm diameter indenter tip positioned above the distal femur mounted on a #10 cap screw head. **(Bottom)** Digital μCT images below the epiphyseal region taken of the same distal femur from a representative 12 week old *Camkk2*$^{-/-}$ mouse before and after direct blunt punch testing. The strength data were determined from only the initial penetration of the punch to avoid artifact from contact with the cortex at deeper penetration as can be seen in the figure. Mouse cohorts analyzed for

strength data are 12 week old WT and *Camkk2*$^{-/-}$ mice (n=11 each), 32 week old saline or ST-609 treated mice (n=9 each) and 32 week old *Camkk2*$^{-/-}$ mice (n=6). **(D)** Average trabecular compression indentation strength ± standard deviation measurements of the trabecular bone from indicated mouse cohorts calculated in MPa are shown. Statistical comparisons among the cohorts were performed using single factor ANOVA followed by post-hoc *t*-test and Bonferroni correction for pair-wise comparisons. Differences with *p* -values < 0.05 were deemed significant and denoted as * = p<0.05; ** = p<0.01; *** = p<0.001 and **** = p<0.0001.

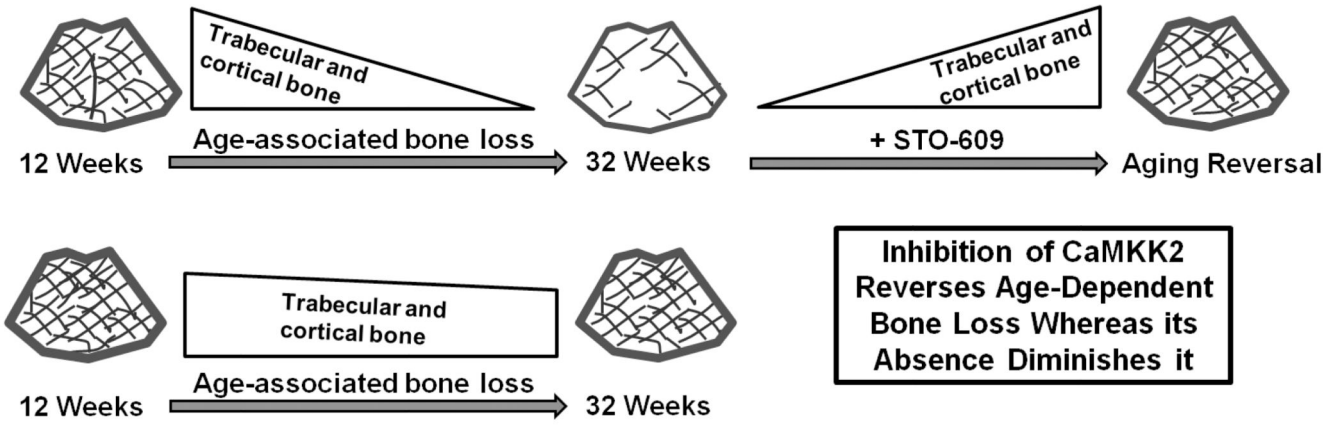

Figure 4. Model: Pharmacological inhibition of CaMKK2 reverses age-associated bone loss in WT mice while its genetic loss attenuates it

From 12 to 32 weeks of age, male WT mice suffer a significant decline in trabecular bone volume, microarchitecture, strength as well as cortical bone strength. Acute inhibition of CaMKK2 in the 32 week old mice through a 6 week treatment with STO-609 stimulates new bone formation in these mice and significantly increases trabecular bone volume, microarchitecture, strength as well as mid-shaft geometry and cortical bone strength to levels observed in 12 week old WT mice. Moreover, regardless of age, the *Camkk2*$^{-/-}$ mice possess significantly elevated bone mass and strength compared to age-matched WT mice. Whereas they undergo age-associated bone loss albeit smaller and often non-significant; the trabecular bone volume, microarchitecture, strength as well as cortical bone strength values are still significantly higher in 32 week old *Camkk2*$^{-/-}$ mice than age-matched WT mice, implying that the chronic absence of CaMKK2 attenuates the deleterious effects of age on bone.

Table

Femur Mid-Shaft Geometry

	Femur mid-diaphysis				
	WT			*Camkk2* $^{-/-}$	
	12W	**32W-Saline**	**32W + STO-609**	**12W**	**32W**
Mediolateral inner diameter (mm)	1.33 ± 0.05	1.27 ± 0.08	1.44 ± 0.11	1.5 ± 0.1	1.35 ± 0.08
Mediolateral outer diameter (mm)	1.84 ± 0.05	1.66 ± 0.04	1.86 ± 0.12	2.0 ± 0.14	1.84 ± 0.15
Dorsoventral inner diameter (mm)	0.87 ± 0.04	0.78 ± 0.07	0.9 ± 0.06	1 ± 0.03	0.9 ± 0.06
Dorsoventral outer diameter (mm)	1.3 ± 0.07	1.2 ± 0.07	1.5 ± 0.03	1.5 ± 0.03	1.34 ± 0.02
Crosssectional area moment of inertia (mm^4)	0.157 ± 0.04	0.112 ± 0.03$^{*\#}$	0.155 ± 0.03$^{*@}$	0.232 ± 0.04$^{**\sim}$	0.17 ± 0.02$^{**\sim}$
Cortical bone thickness (mm)	0.46 ± 0.05	0.4 ± 0.05	0.43 ± 0.04	0.5 ± 0.04	0.47 ± 0.06

Statistical significance is denoted as:

* - p-value < 0.05;

** - p-value <0.01.

$^{\#}$ - compared to 12W WT;

$^{@}$ - compared to 32W-saline;

$^{\sim}$ - compared to respective age-matched WT cohorts.